IAC-17-C4.6.8

STATION-KEEPING WITH AN ELECTROSPRAY PROPULSION SYSTEM FOR LOW LUNAR POLAR MISSION ON A 6U CUBESAT

Michele Benetti[1], Camilla Colombo[1], Charlie Ryan[3]

[1] Politecnico di Milano, Dep. of Aerospace Science and Technology, Milano, Italy; camilla.colombo@polimi.it
[3] University of Southampton, Astronautics Research Group, Southampton, UK

The suitability of electrospray propulsion for station keeping of a 6U CubeSat in lunar orbit is assessed. Lunar CubeSat missions are of interest with the launch of several CubeSat on-board the first Space Launch System launch. For interplanetary CubeSat missions, electrospray thrusters have the potential to provide good performance within the nanosat constraints. An electrospray thruster electrostatically accelerates charged droplets or ions, producing small thrusts at high specific impulse. To investigate the feasibility of using an electrospray system for station keeping, the maximum variation of orbital parameters for lunar polar orbits are evaluated. This was completed with the High Fidelity Orbit Dynamics (HiFiODyn), developed at Politecnico di Milano for orbit long-term propagation. The Gauss-planetary equations were integrated over time considering a 100 x 100 Lunar Prospector 165 x 165 spherical harmonic solution (LP165P) gravity model of the Moon and both the Earth and the Sun considered as third body. Without any propulsion system over a period of 70 days typical variations of orbital elements for low quasi-circular lunar polar orbits were assessed. Moreover, the evolution of different orbits was evaluated, with varying eccentricity and inclination and fixed initial epoch, semi-major axis, argument of perigee, longitude of the ascending node and mean anomaly. Maps of the maximum variation of all the Keplerian elements for these orbits were created. These maps have eccentricity that varies between 0.01 and 0.045 and inclinations that span from 85 to 95 degrees. A micro-electrospray propulsion system being developed at the University of Southampton was then considered in the simulation to assess its ability to keep a stable orbit. Both power and mass/volume were constrained for a 6U CubeSat using a model of a micro-electrospray thruster that allows an estimate of the thrust and the specific impulse. With thrust values of between 0.3 mN and 1 mN and specific impulse value of between 1000 s and 4000 s some different manoeuvres were performed to assess the ability of the propulsion system to maintain a prefixed value of an orbital parameter. The same maps were created with and without the electrospray propulsion system considered. It is demonstrated that the micro-electrospray system makes a significant difference to the variation with time of the polar orbit when a proper manoeuvre is used considering also that the thrust value of such system is much lower than typical perturbations of these low polar orbits.

Keywords: CubeSat; Moon; Electrospray propulsion; Orbit design; Orbit perturbations

Nomenclature

a	*= semi-major axis*
a_0	*= initial semi-major axis*
i	*= inclination*
i_0	*= initial inclination*
e	*= eccentricity*
e_0	*= initial eccentricity*
ω	*= argument of perigee*
ω_0	*= initial argument of perigee*
Ω	*= right ascension of the ascending node*
M	*= mean anomaly*
m	*= satellite mass*
m_0	*= initial satellite mass*
m_p	*= propellant mass consumption*
I_{sp}	*= specific impulse*
T	*= thrust*
T_{em}	*= thrust per emitter*
N_{em}	*= number of emitters required for a desired T*
P	*= power required for a desired T*
g_0	*= standard gravity*
r	*= magnitude of the satellite position vector with respect to the centre of the reference system*
h	*= magnitude of the satellite angular momentum*
θ	*= true anomaly*
μ	*= standard gravitational parameter*
a_h	*= component of the perturbing acceleration along the h-axis*

a_n = *component of the perturbing acceleration along the n-axis*
a_t = *component of the perturbing acceleration along the t-axis*
p_h = *component of the perturbing acceleration along the h-axis due to the thrust action*
p_n = *component of the perturbing acceleration along the n-axis due to the thrust action*
p_t = *component of the perturbing acceleration along the t-axis due to the thrust action*
$\boldsymbol{p}$ = *perturbing acceleration due to the thrust action*
sgn = *sign function*
q/m = *charge-to-mass ratio of charged particles emitted*
β_n = *fraction of current carried by nth species with respect the total current*
V = *applied voltage*
V_{em} = *emitter voltage*
V_{acc} = *accelerator voltage*
1U = *10 cm · 10cm · 10 cm*
ε = *ratio of the charge-to-mass ratio of species 1 over the charge-to-mass ratio of the species 2*
η_0 = *overall efficiency of the ejected beam*
$\dot{m}$ = mass flow rate of the ejected beam

Acronyms/Abbreviations

ILIS	Ionic Liquid Ion Source
SLS	Space Launch System
RAAN	Right Ascension of the Ascending Node
LLO	Low Lunar Orbit
HiFiODyn	High-Fidelity Orbital Dynamics
LP	Lunar Prospector
LP165P	Lunar Prospector 165 x 165 spherical harmonic solution
DE	Developmental Ephemeris
EP	Electric Propulsion
EMI-BF_4	1-ethyl-3-methyl-imidazolium tetrafluoroborate
PIR	Pure Ionic Regime

1 Introduction

CubeSat were born as a result of a project started in 1999 to reduce cost of satellites by standardising its production, producing small satellites that can be injected in orbit as a piggyback or directly from the International Space Station. Since then the vast majority of CubeSat have flown without any propulsion system, even if the last decade has seen significant advances in the development of micro-propulsion systems. Indeed, new thruster systems are approaching flight demonstration, with some of them are already available in the market [1]-[4]. In particular, Electric Propulsion (EP) systems are good candidates for CubeSat missions requiring larger changing in velocity and which do not require fast impulsive manoeuvres [5]. Nevertheless, technologies like plasma thrusters suffer when scaled-down, with a consequent reduced lifetime and efficiency. Electrospray thrusters can though be easily miniaturised and yet still have high efficiency and specific impulse. This motivates the development of a new type of electric propulsion technology: ion electrospray propulsion [6].

Regarding ion electrospray propulsion technology, the physical processes that govern the beam composition of ionic liquids in a Ionic Liquid Ion Source (ILIS) is not well understood yet, resulting in ILIS's at times producing ion, droplets, or a mixture of both. It is then important to rely on beam composition experimental data, especially given the large performance variation when ions are emitted (I_{sp} ~ 1000's seconds) compared to droplets (I_{sp} ~ 100's seconds). Data of ILIS beam composition can be found in literature since the last few years; several research groups have in fact targeted high current density, passively fed ILIS's which can provide 10's of μN of thrust per cm^2. Depending on the type and geometry of ILIS emitter structures, each emitter may support multiple emission sites and yield from 0.1 to > 5 μA of emission current per emitter [7]. The main parameters that drive the beam composition, and therefore the performance, of an electrospray propulsion system are the emitter size, the propellant liquid, and the emitter voltage. Moreover, Courtney and Shea have analysed the correlation between the reservoir pore size diameter and the beam composition, highlighting a strong influence of the back pressure (due to which the liquid enters the emitter) onto the beam composition [8]. Electrospray propulsion systems are now approaching the market for the first time, encouraging further research to optimise these systems. The first flight electrospray thruster was created by Busek Co. Inc. for the

Lisa Pathfinder mission launched on 3 December 2015 [9] and Busek are now developing further electrospray thruster systems; other electrospray propulsion units are also under development by Accion [3]. In addition, thanks to the renewed interest in the exploration of the Moon [18]-[22], electrospray propulsion technology could enhance the manoeuvre capability of nano-satellites; this is strongly desired especially for interplanetary mission.

The first aim of this study is then to assess if an electrospray propulsion system is effective for station keeping orbits at the Moon for a future lunar mission with the constraints of a CubeSat. To investigate this possibility, an electrospray thruster model was created relying on experimental results available in literature [27],[28]. Useful information on the feasibility of such a propulsion system for 6U CubeSat to the Moon can be obtained.

In the last decade the exploration of the Moon is again of interest, partly due to the presence of water but also because it represents an optimal test-bed for advanced CubeSat, both to analyse the ability of these nano satellites to perform a scientific mission and to validate new technologies [10]. Lunar orbits are extremely perturbed by the Moon's gravity field and third body perturbations, therefore a propulsion system is required to stabilise the satellite's dynamics. For Low Lunar Orbits (LLOs) lower than 750 km altitude the non-uniform gravity field of the Moon is the main driver of the orbit dynamics. Folta and Quinn studied low lunar frozen orbits [11], finding that, with an accurate modelling, orbital elements exhibit a pattern that can drive the overall mission design. A selection of stable lunar orbits can reduce or even eliminate the need for station keeping, while maintaining an orbit that allows science or communication and navigation. Moreover, they found that frozen orbits are all near circular (eccentricity < 0.05, while their altitude lies at about 100 km altitude). Lara extended the study of these lunar frozen orbits using a more accurate model than previous works: a higher zonal degree truncation of the Moon gravity potential up to the 100th order, superimposed to the Earth mass-point attraction. The resulting diagrams allow the selection of low altitude near-circular lunar frozen orbits [12]. Perez studied the influence of the choice of initial Right Ascension of the Ascending Node (RAAN) and inclination and concluded that an analysis performed with high-fidelity orbital propagation is a fundamental asset for future lunar missions. In fact, a limited set of orbital parameters define boundaries between stable and unstable orbits [13]. The study of lunar orbits for a particular set of initial conditions, with high fidelity model, can then be useful to understand the dynamics behaviour of LLOs.

The second aim or our work is then to define an operational orbit at the Moon such that Moon observation can be performed for an extended time. To study the stability of low-altitude operational orbits at the Moon, the maximum variation in orbital parameters for a set of low lunar quasi-circular polar orbits is calculated for both the case in which the satellite's dynamics is free and the case in which an electrospray propulsion system is used to control the satellite's dynamics. In this second case, the values of thrust and specific impulse are derived a simple electrospray propulsion system model taking into consideration CubeSat constraints. As a result, a discussion on the applicability of an electrospray propulsion system for a 6U CubeSat to the Moon is given.

2 CubeSat orbital dynamics and control

2.1 Orbital dynamics model

The High-Fidelity Orbital Dynamics (HiFiODyn) suite developed at Politecnico di Milano can predict the orbital evolution of a satellite with high-fidelity dynamics. The HiFiODyn suite was developed within the FP7 EU framework in the Marie Sklódowska-Curie Actions [14]. It was originally designed together with a semi-analytical propagator PlanODyn for the long-term propagation of highly elliptical orbits and satellite disposal from such

orbits by enhancing the effect of natural perturbations [15]. HiFiODyn has been later extended to treat also medium Earth orbits, low Earth orbits [16], heliocentric orbits and Libration Point Orbits [17] and now the Moon's Orbits with this work. With this tool, maps representative of the behaviour of LLO (approximately lower than 125 km altitude) in polar region were created. These maps are useful to understand the strong instability of such orbits, looking especially at the maximum variation of orbital parameters over a reference period of 70 days, which is a suitable duration of a CubeSat mission around the Moon [18]-[22]. The dynamics of the satellite is here studied assuming that the satellite is already injected in an orbit around the Moon, and considering as perturbing acceleration both the effect due to the non-uniform gravity field of the Moon and the third body effect of both the Earth and the Sun. In particular, a 100 degree 100 order LP165P (Lunar Prospector 165 x 165 spherical harmonic solution) was used as gravity model, while DE421 ephemerides were used to calculate the position of the Earth and the Sun with respect the Moon. LP165P still suffers by the lack of farside tracking [23]; however the Lunar Prospector (LP) models should accurately predict any circular orbit for inclinations greater than 80° [24], that is the case investigated in this paper (see Subsection 2.2). DE421 as ephemerides and LP165P as gravity model were chosen to assure a detailed description of the motion of a satellite orbiting around the Moon.

2.2 Low lunar orbits

The two-body equations of relative motion between two objects is based on the assumption that there are only two objects in space, and that they spherically symmetric gravitational fields are the only source of interactions between them. If this ideal case is considered, Keplerian orbits are then the solution of the two-body equations. This is clearly an ideal scenario; for real space other forces can influence the dynamics of the two-body problem; they are known as perturbations.

For the discussion here presented, only the main perturbations acting on a body that orbits around the Moon were considered; they are due to the non-uniform gravity field of the Moon and the third body effect of both the Earth and the Sun [11],[29]. Solar radiation pressure is not considered in the work here presented. For lunaraltitudes lower than approximately 750 km a high order-high degree potential gravity model must be used to obtain a correct description of the motion; the lower the altitude the more detailed the gravity model has to be if a reliable orbital evolution is required.

The perturbation due to the non-spherical shape of the Moon was integrated in the Gauss-planetary equations:

$$\begin{aligned}
\frac{d\Omega}{dt} &= \frac{r\sin(\omega+\theta)}{h\sin(i)}a_h \\
\frac{di}{dt} &= \frac{r\cos(\omega+\theta)}{h}a_h \\
\frac{d\omega}{dt} &= \frac{1}{ev}\left[2\sin(\theta)a_t + \left(2e+\frac{r}{a}\cos(\theta)\right)a_n\right] \\
&\quad - \frac{r\sin(\omega+\theta)\cos(i)}{h\sin(i)}a_h \\
\frac{da}{dt} &= \frac{2a^2v}{\mu}a_t \\
\frac{de}{dt} &= \frac{1}{v}2\left(e+\cos(\theta)a_t\right) - \frac{r}{a}\sin(\theta)a_n \\
\frac{dM}{dt} &= n - \frac{b}{eab}\left[2\left(1+\frac{e^2r}{p}\sin(\theta)a_t\right) + \frac{r}{a}\cos(\theta)a_n\right]
\end{aligned} \tag{1}$$

The perturbing acceleration $\mathbf{a} = \{a_t, a_n, a_h\}$, expressed in the *t*-*n*-*h* body-fixed (i.e. fixed with the satellite) reference frame, can represent both the perturbing acceleration due to the effects of orbit perturbations, or the control acceleration of the electrospray given in Eq. (2). In this frame the *t*-axis is directed as the tangent to the motion of the satellite, the *h*-axis is in the direction of the angular momentum, and the *n*-axis is directed in the orbit plane, normal to the *t*-axis (inward). The set of equations (1) are numerically integrated to get the evolution of the orbital

elements in time. From there, maps representative of the stability of the orbit can be created.

Among all the possible initial orbits that could be chosen for orbit evolution analysis, a frozen orbit was firstly studied. Indeed, selecting these orbits can reduce or even eliminate the need of station keeping due to their nature. Low lunar quasi-frozen orbits were considered. The assessment of maximum differences in Keplerian elements for both frozen orbits and non-frozen orbits, chosen in the neighbourhood of frozen orbit conditions, were calculated to meet the mission requirements.

To locate frozen orbits inclination-eccentricity diagrams of frozen orbits were used; they are available in literature with different level of accuracy (see Refs. [11][12][29]). These diagrams, for a given semi-major axis and for a value of argument of perigee of 90° or 270°, give the value of eccentricity and inclination that provide the lunar frozen orbit condition. Three values of semi-major axis (required for the frozen orbit conditions) were then considered as initial conditions for the limited set of orbits analysed here, and are listed in Table 1.

Table 1. Set of initial conditions chosen for the assessment of typical variation of low quasi-circular lunar polar orbits.

Set name	a_0 [km]	ω_0 [deg]
LLO 1	1863	270
LLO 2	1838	270
LLO 3	1813	270

For these three values of initial semi major axis a_0 and initial anomaly of the perigee ω_0, eccentricity-inclination diagrams indicate that polar frozen orbits exist only for ω_0 = 270 deg and eccentricity that span from 0 to 0.06 as maximum. This region was then simulated for a range of initial inclinations within the range $85 < i < 95$ degrees. More precisely, for these three prescribed set of initial conditions, the initial orbit inclination was varied between 85 deg and 95 deg with step of 1 deg. The eccentricity instead was varied from the value of 0.01 to the value of 0.045 in steps of 0.005 for the first two set of initial parameter in Table 1, and the same was done for the third orbit but with the upper value of eccentricity equal to 0.041 instead of 0.045 to avoid an initial perigee radius lower than the Moon's radius. Henceforth the first set of conditions in Table 1 will be referred as LLO 1, the second set as LLO 2 and the third one as LLO3.

2.3 Station-keeping

At the current stage of this work, as the optimal control problem for feedback stabilisation of a quasi-stable orbit has not yet been implemented, a pre-defined manoeuvre was implemented to maintain a stable initial inclination i_0; the quasi-optimal law of Table 1 in Ref. [25], here reported, was selected to achieve this goal.

$$\begin{aligned} a_{c,t} &= 0 \\ a_{c,n} &= 0 \\ a_{c,h} &= \left(\bar{a}_c\left(\sin\left(sgn\left(\cos\left(\omega+\theta\right)\right)\frac{\pi}{2}\right)\right.\right. \end{aligned} \tag{2}$$

$\mathbf{a}_c = \left\{a_{c,t}, a_{c,n}, a_{c,h}\right\}$ are the components of the control acceleration along the *t*, *n*, *h*-axis due to the thrust action, while $\bar{a}_c$ is the magnitude of the control acceleration, which is calculated from the constant thrust *T* and the variable mass of the spacecraft as will be shown in Eq. (3). This particular manoeuvre was implemented in the hypothesis that the electrospray propulsion system considered is always able to thrust in the optimal direction, i.e. along the *h*-axis with direction depending on the sign function of Eq. (2). The case here considered is then ideal because the electrospray propulsion system it is not able to performed any instantaneous thrust vectoring control. Nevertheless, this type of station-keeping is one of the most expensive in terms of propellant mass, that is a key parameter in the design of a CubeSat propulsion system, motivating this choice.

EP typically increases the payload mass fraction when used as main propulsion with respect to the case of

chemical propulsion, reducing the propellant required to perform given orbital manoeuvres [25]. Nevertheless, EP systems have low thrust values with respect to chemical ones. If a precise control of the orbit is required and strong perturbation effects are present, the low thrust value makes EP systems unattractive for station-keeping. Then, if an electrospray propulsion system is used on a CubeSat for an orbit around the Moon, the low value of thrust could not be high enough to control the dynamics of the orbit. A low-thrust manoeuvre law is then needed to explore this scenario. When low-thrust values, typical of electrospray propulsion system, are used to perform such a manoeuvre, the action of the thruster to the satellite's dynamic can be considered as a perturbation acting on the satellite and so it can be integrated by means of Gauss-planetary equations (1). In this way, the ability of the thruster to counteract perturbation on the satellite's dynamics can be assessed.

The mass of the satellite was also considered as variable whose dynamics is reported in Eq. (3), and the resulting mass consumption is used to estimate, by means of the Tsiolkovsky's rocket equation [30], the velocity increment corresponding to the performed manoeuvre.

$$\frac{dm}{dt} = -\frac{T}{I_{sp} g_0} \tag{3}$$

The thrust value T is considered as constant during the entire manoeuvre.

3 Electrospray system dimensioning

No CubeSat have yet been launched to the Moon; various missions are though under development, and the system design of these can be fed into the constraints considered here. Power budget, mass and volume typical of these missions were used as constraints in the electrospray thruster model in order to guess maximum value of power consumption, number of emitters, thrust value and specific impulse of the electrospray propulsion system considered.

3.1 Design constraints

Based upon a survey of current lunar CubeSat missions a 6U CubeSat has enough volume to carry all the instrumentations necessary for a mission around the Moon. The 6U size was then chosen also for this study as the minimum CubeSat's. Among the proposed CubeSat missions to the Moon, the Lunar Water Distribution (LwaDi) [26] mission, which mounts a μPPT propulsion system, was taken as reference to retrieve information related with subsystem allocation. According to [26], the constraints considered for the propulsion system are 1.5 kg as maximum wet mass, 40 W of power always available for the propulsion system, and 1.5 U of maximum volume.

3.2 Electrospray propulsion system

In its simplest form an electrospray propulsion system, represented in Fig. 1, is composed of:

- an emitter in which the liquid is fed. Electrified particles are ejected from its apex;
- an extraction electrode aligned with the emitter that provides the energy necessary for the emission of particles;
- a reservoir connected with the emitter where a conductive liquid propellant is stored;
- an additional accelerator electrode that further accelerates ejected species, allowing higher thrust and specific impulse.

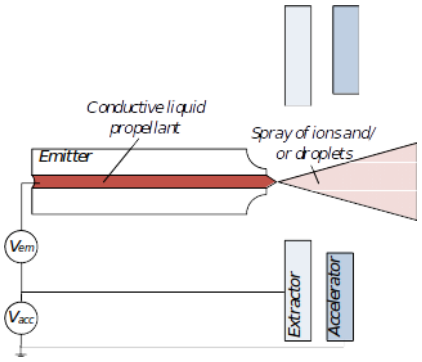

Fig. 1. Scheme of an electrospray propulsion system [31]. Accelerator is grounded.

3.3 Electrospray thruster model

A thruster model of an electrospray propulsion system was created relying mainly on experiment results presented in Ref. [27],[28]. In fact, the ILIS device is still under study at the University of Southampton and a thruster model should be created relying on further experimental results if a reliable thruster model is desired. By doing so, two feasible values of thrust and specific impulse (feasible with constraints of Subsection 3.1) were calculated from the electrospray thruster model and used in the manoeuvre discussed in Subsection 2.3: 0.3 mN and 1 mN as thrust and 1000 s and 4000 s as specific impulse. When EMI-BF_4 (1-ethyl-3-methyl-imidazolium tetrafluoroborate) is used as propellant, these two values of thrust can be reached both with a mixed-mode or a Purely Ionic Regime (PIR), but for specific impulses that differ by a great amount depending on the operative condition: mixed-mode is characterised by a lower specific impulse (1000 s) with respect the one of PIR (4000 s). In particular two ejected beams were considered, one representative of a typical mixed-mode and one of a PIR when the ionic liquid EMI-BF_4 is used as propellant [27][28]; they are summarised in Table 2.

Table 2. Beam composition considered in the thruster model. Species 1 is, for both operative conditions, the monomer $[EMI]^+$, while species 2 is represented by the dimer $[EMI\text{-}BF_4][EMI]^+$ for the PIR and is represented by a typical droplet size for the mixed-mode. PIR and mixed-mode differ also for the emitted current carried by the two species β.

Case	$(q/m)_1$ [C/kg]	$(q/m)_2$ [C/kg]	β_1	β_2
PIR	$8.679 \cdot 10^5$	$3.121 \cdot 10^5$	0.5	0.5
Mixed-mode	$8.679 \cdot 10^5$	$4.818 \cdot 10^3$	0.9	0.1

Values of charge-to-mass (q/m) ratio are calculated using the molar mass of molecules. β_1, and as direct consequence β_2, in Table 2, are instead a common value found experimentally [27],[28]. Other regimes are also possible, for example a PIR regime where only $[EMI]^+$ composes the beam, or also a droplet mode where no ions are present in the ejected species; but as they are not easily observed in experiments they were not considered in the thruster model presented here.

Accordingly to results presented in Ref. [28], using EMI-BF_4 PIR is obtained for different values of emitter voltage, V_{em} (for the discussion here presented let the emitter voltage V_{em} be the potential difference between the emitter and the extractor). Two values of the emitter voltage V_{em}, and then two of the emitter current I_{em}, for each regime considered (PIR and the mixed mode), are now assumed, accordingly to experimental results in Ref. [27]. One is representative of the minimum emitted current and the other of the maximum one for the regime under consideration. These four values are needed to model the possible performances of the electrospray propulsion system for the mixed regime and PIR considered. These values are listed in Table 3: "min" and "max" refer respectively to the minimum and maximum assumed emitter current I_{em}. Higher and lower values of I_{em} with respect to the one listed in Table 3 are also possible, depending on V_{em} but as conservative assumption, the highest and lowest values experimentally recorded were not here considered.

Table 3. Maximum and minimum emitted current conditions assumed in this work. The 5 μA I_{em} value represent the minimum emitted current value considered while the 20 μA value represent the maximum one.

Case	V_{em} [V]	I_{em} [μA]
PIR min	2000	5
PIR max	2200	20
Mixed-mode min	1600	5
Mixed-mode max	1900	20

Furthermore, for these 4 cases, an accelerator voltage V_{acc} was also considered (let the accelerator voltage V_{acc} be the potential difference between the extractor and the accelerator now considered) and added to V_{em}. V_{acc} was

arbitrary varied from 0 V to 3000 V for the 4 cases under consideration in Table 3. Higher V_{acc} are also possible, but as it will be explained in Section 4.3, they might not be feasible with the power budget of a typical 6U CubeSat, depending on the thrust considered.

In the hypothesis that only two species compose the ejected beam, as in this case, the specific impulse (let the specific impulse of the ejected beam be $I_{sp\text{-}mix}$) can be calculated using equation [32]:

$$I_{sp-mix} = I_{sp-1}\frac{\sqrt{\varepsilon}-\left(\sqrt{\varepsilon}-\varepsilon\right)\beta_1}{1-\left(1-\varepsilon\right)\beta_1} \tag{4}$$

where $I_{sp\text{-}1}$ is the specific impulse of the species with largest charge-to-mass ratio q/m of the charged particles emitted (EMI+ for the case here considered) and ε is the ratio of the charge-to-mass ratio of species 1 over the charge-to-mass ratio of the species 2. β_1 is the fraction of current carried by nth species with respect the total current. $I_{sp\text{-}1}$ can be calculated using Eq. (5).

$$I_{sp-1} = \frac{1}{g_0}\sqrt{2V\left(\frac{q}{m}\right)_1\eta_0} \tag{5}$$

In Eq. (5), V is *the* applied voltage (defined as the potential difference between emitter and accelerator), q/m is the charge to mass ratio of species 1, while η_0 is the overall efficiency of the ejected beam, that is equal to one in an ideal case where no losses are present in the final energy content of the beam (for a discussion of efficiencies of an electrospray propulsion system the reader can refer to Ref. [33]). With $I_{sp\text{-}mix}$ known, the last parameter needed to calculate the thrust of the ejected beam is the mass flow rate $\dot{m}$:

$$\dot{m} = \frac{I_{em}\beta_1}{\left(q/m\right)_1} + \frac{I_{em}\beta_2}{\left(q/m\right)_2} \tag{6}$$

The thrust obtained from one emitter T_{em} can then be calculated by means of Eq. (7):

$$T_{em} = \dot{m}g_0 I_{sp-mix} \tag{7}$$

If a desired value of thrust $\bar{T}$ is desired, the number of emitters required are easily calculated as $\bar{T}$ over T_{em}. The power P needed to obtain the desired $\bar{T}$ is instead calculated as function of the number of emitters N_{em} by using $P = I_{em}VN_{em}$.

4 Results

4.1 Low Lunar Orbits

Maximum difference of the altitude and the inclination parameter for LLO1, LLO2, and LLO3 in the region of inclination-eccentricity considered are presented in Fig. 2. Impact conditions with the Moon's surface were observed for LLO2 and LLO3, considering as an impact the condition at which the altitude is equal to zero neglecting then Moon's mountains. All these impacts are observed after 55 days and the initial conditions that drive to these impacts are listed in Table 4 and Table 5.

Table 4. Impact and non-impact conditions for LLO2. The symbol "●" indicates that no impacts occur; the symbol "x" indicates that impact occur.

e/*i*	85°	86°	87°	88°	89°	90°	91°	92°	93°	94°	95°
0,010	●	●	●	●	●	●	●	●	●	●	●
0,015	●	●	●	●	●	●	●	●	●	●	●
0,020	●	●	●	●	●	●	●	●	●	●	●
0,025	●	●	●	●	●	●	●	●	●	●	●
0,030	●	●	●	●	●	●	●	●	●	●	●
0,035	●	●	●	●	●	●	x	x	●	●	●
0,040	●	●	●	●	●	x	x	x	●	●	●
0,045	●	●	●	●	●	x	x	x	●	●	●

Table 5. Impact and non-impact conditions for LLO3. The symbol "●" indicates that no impacts occur; the symbol "x" indicates that impact occur.

e/*i*	85°	86°	87°	88°	89°	90°	91°	92°	93°	94°	95°
0,010	●	●	●	●	x	x	x	x	x	●	●
0,015	●	●	●	●	x	x	x	x	x	●	●
0,020	●	●	●	●	x	x	x	x	x	●	●
0,025	●	●	●	●	x	x	x	x	x	●	●
0,030	●	●	●	●	x	x	x	x	x	●	●
0,035	●	●	●	●	x	x	x	x	x	●	●
0,040	x	x	x	x	x	x	x	x	x	x	x
0,041	x	x	x	x	x	x	x	x	x	x	x

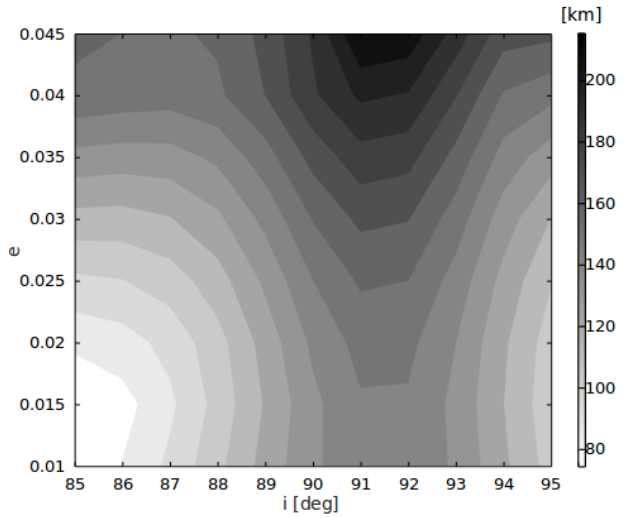

a) LLO1: maximum variations of altitude

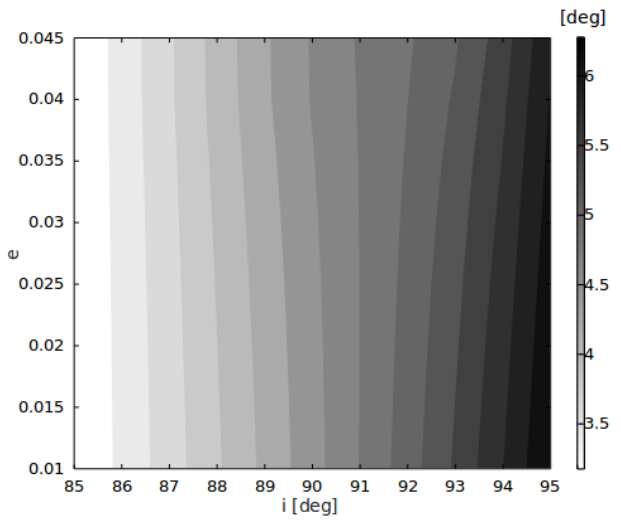

b) LLO1: maximum variations of inclination

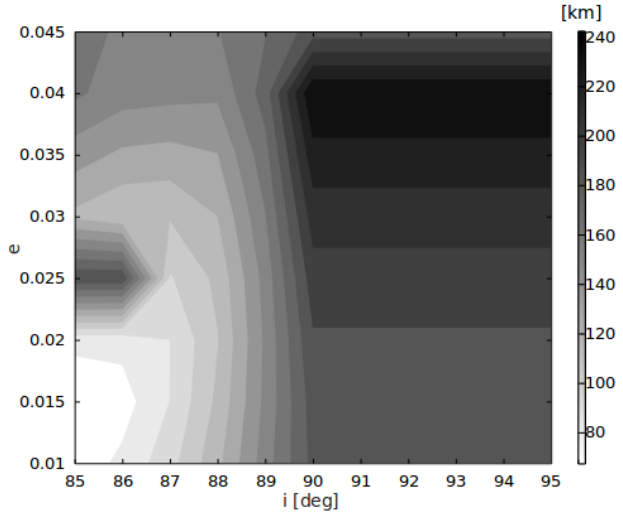

c) LLO2: maximum variations of altitude

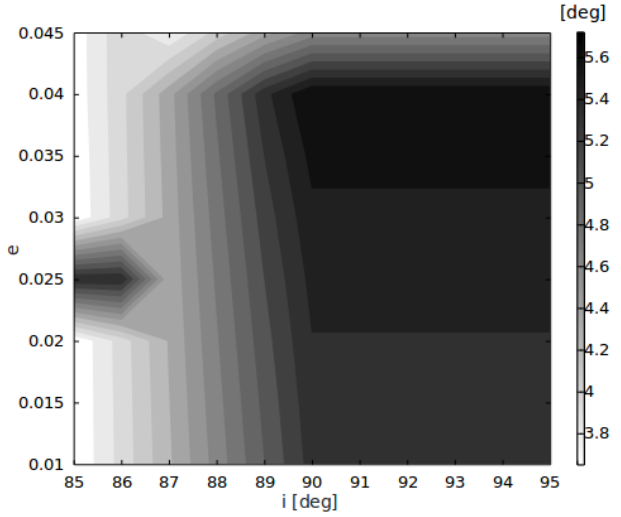

d) LLO2: maximum variations of inclination

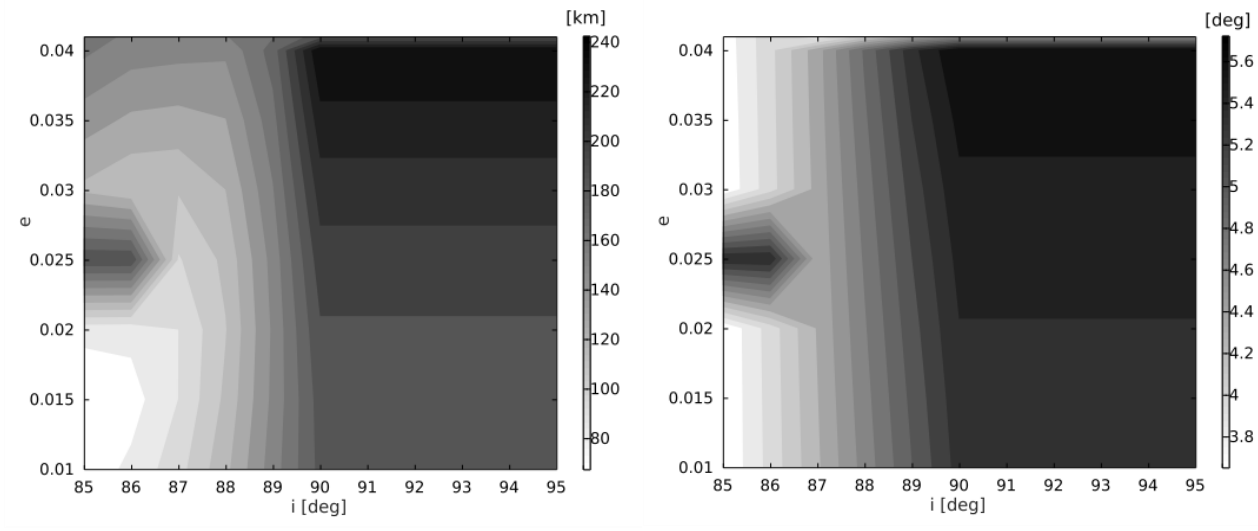

e) LLO3: maximum variations of altitude **f) LLO3: maximum variations of inclination**

Fig. 2. Low Lunar Orbits: iso-lines representative of the maximum variations of the altitude and the inclination over a period of 70 days depending on the initial eccentricity e_0 and the initial inclination i_0 considered for (a) LLO1, (b) LLO2, and (c) LLO3.

4.2 Station-keeping

The ability of the electrospray propulsion system to control the satellite dynamics was evaluated for LLO 1 by recreating the same kind of maps of Fig. 2 considering the manoeuvre as active. Results of this new simulation are now presented in Fig. 3.

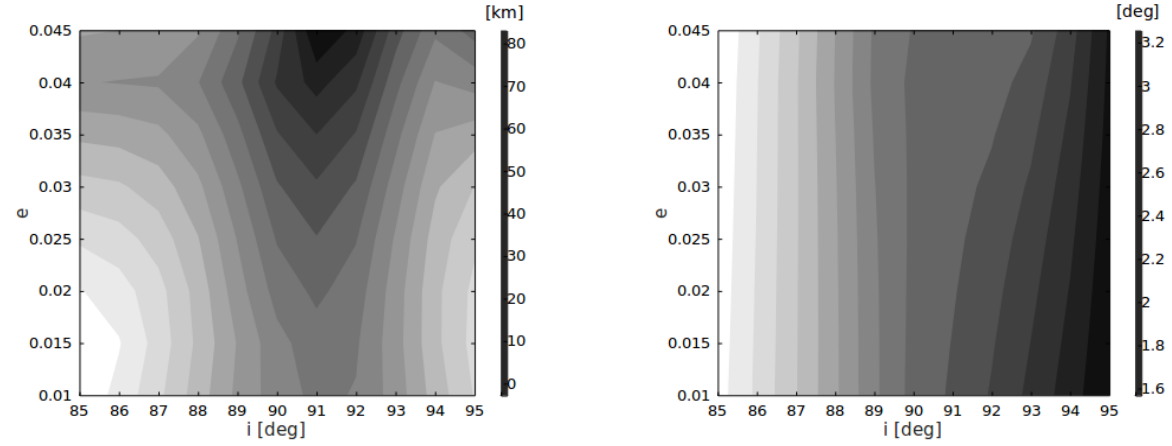

a) Maximum variations of altitude with T = 0.3 mN **b) Maximum variations of inclination with T = 0.3 mN**

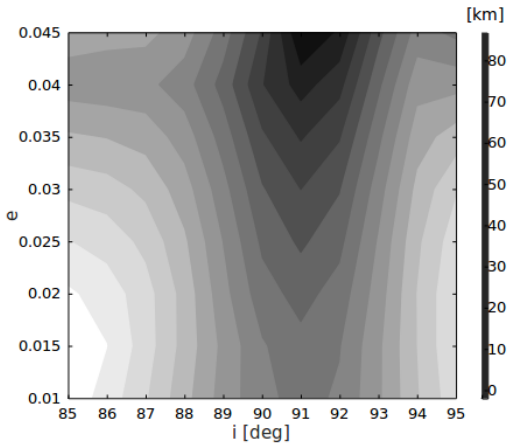

c) Maximum variations of altitude with T = 1 mN

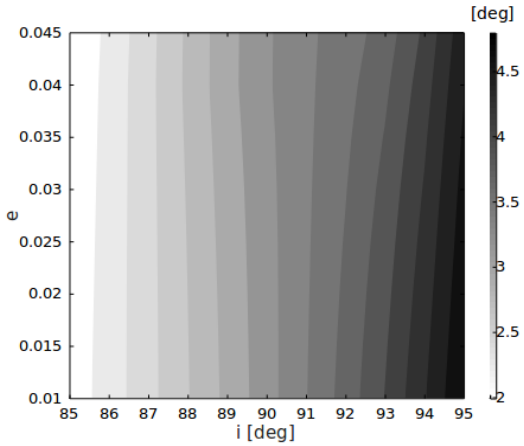

d) Maximum variations of inclination with T = 1 mN

Fig. 3. LLO 1: iso-lines representative of maximum variations of the altitude and inclination over a period of 70 days depending on the initial eccentricity e_0 and inclination i_0 considered with a thrust T of 0.3 mN and 1 mN.

For these manoeuvres, the propellant mass m_p was calculated by means of Eq. (3) with an initial mass m_0 of 12 kg. Results of m_p are shown in Table 6, where also the volume occupied by the propellant is shown, considering a density of EMI-BF4 of 1271 kg/m^3 [34].

Table 6. Propellant mass consumption of the manoeuvres performed.

m_p [g]	V_p [CubeSat Units]	V_p [cm^3]	T [mN]	I_{sp} [s]
184.954	0.235 U	235.077	0.3	1000
46.509	0.059 U	59.113	0.3	4000
616.514	0.784 U	783.589	1	1000
157.190	0.200 U	199.788	1	4000

4.3 Electrospray thruster model

With respect to Subsection 3.3, results of the thruster model considered are now presented. In particular specific impulse, number of emitters and power required for 0.3 mN and 1 mN of thrust considered in Table 6 are shown for both PIR and mixed-mode. In Fig. 4, Fig. 5 and Fig. 6, the coloured regions represent the operative conditions of the electrospray thruster considered. Regarding the constraints of mass/volume assumed so far, an electrospray propulsion system being in development at the University of Southampton will explore this scenario.

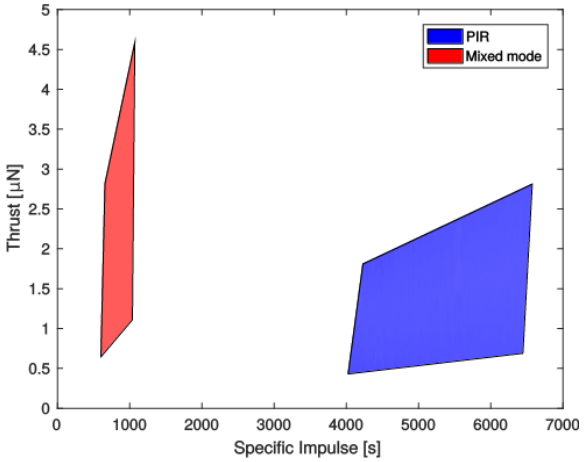

Fig. 4. Thrust obtained from a single emitter. For this figure the top limits are obtained for the maximum emitted current I_{em}, while the bottom limits are obtained for the minimum I_{em}. The left and right limits are set by the minimum and maximum voltage V applied.

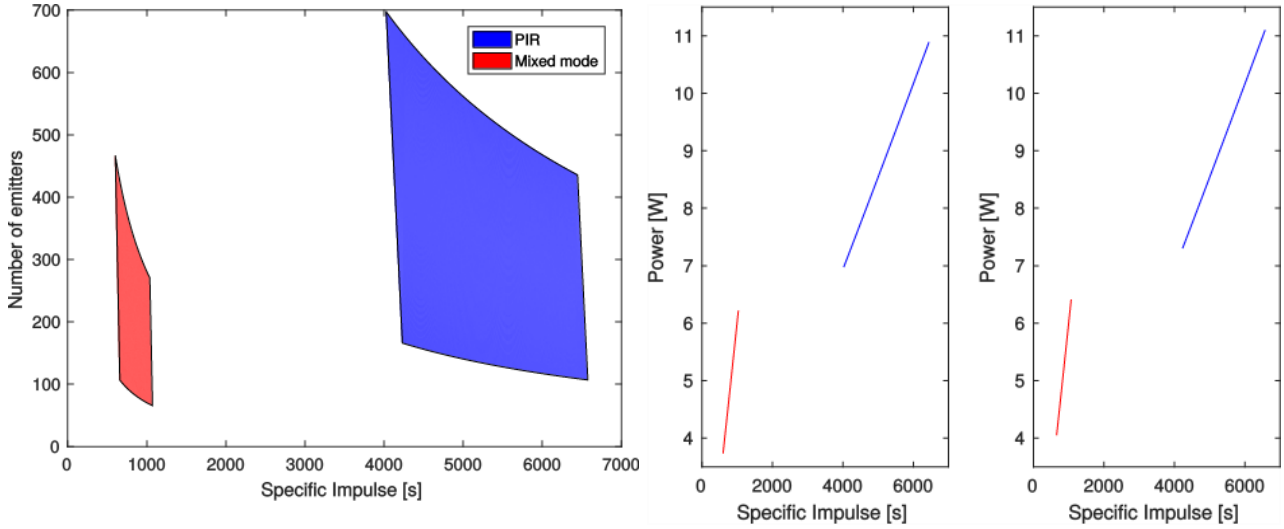

a) Required number of emitter N_{em} for T = 0.3 mN **b) Required power for T = 0.3 mN**

Fig. 5. Number of emitter N_{em} and power required for 0.3 mN of thrust. (A) For this figure the top limits are obtained for the minimum emitted current I_{em} , while the bottom limits are obtained for the maximum I_{em}. (B) The red line is representative of the mixed-mode and blue line of PIR. Figure to the left represent the power required when the minimum I_{em} is obtained; figure to the right represent the required power P when the maximum I_{em} is obtained.

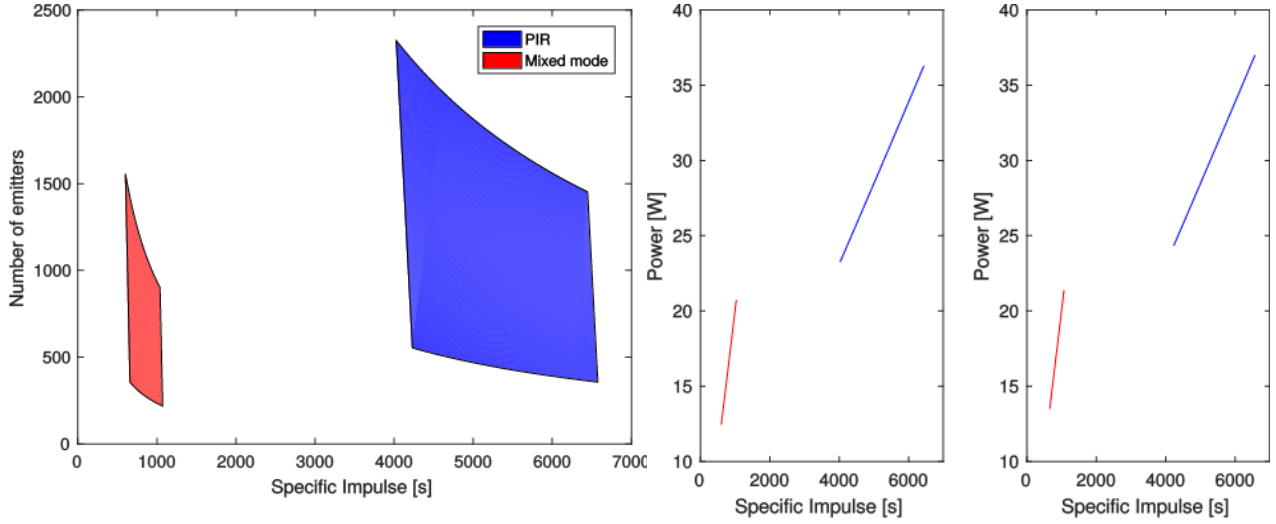

a) Required number of emitter N_{em} for T = 1 mN **b) Required power for T = 1 mN**

Fig. 6. Number of emitter N_{em} and power required for 1 mN of thrust. (A) For this figure the top limits are obtained for the minimum emitted current I_{em} , while the bottom limits are obtained for the maximum I_{em}. (B) The red line is representative of the mixed-mode and blue line of PIR. Figure to the left represent the power required when the minimum I_{em} is obtained; figure to the right represent the required power P when the maximum I_{em} is obtained.

5 Discussion

5.1 Low Lunar Orbits

Fig. 1 confirm that LLOs are extremely perturbed and station-keeping is needed to control the satellites orbital dynamics. This is also highlighted by looking at Table 4 and Table 5. In fact, impacts occurred for some orbits just after 55 days; impacts are located between an initial inclination i_0 of 89 deg and 93 deg. It can also be noted, by looking at these two tables, that impacts are more likely to occur for LLO3 because of a lower initial semi-major axis a_0. Moreover, no symmetry exist in impact condition, with the prograde orbits seeming to be better candidates to avoid impacts with the Moon′s surface.

5.2 Station-keeping

The station-keeping performed is able to reduce maximum variations of the inclination and of the altitude as well (the reader is referred from Fig. 3). This is not straightforward because the manoeuvre implemented acts directly only on the inclination, and not on the altitude. This result suggests that the inclination is a key parameter in the control of low lunar quasi-circular polar orbits. An optimal control law will be implemented as a future work.

5.3 Electrospray thruster model

With a maximum of 40 W available for the propulsion system, that is a limit case nowadays, it is clear than the thrust value of 0.3 mN considered in the thruster model (see Subsection 3.3) can be enhanced to greater values (see Fig. 5) . In addition, a greater value of thrust can be desired to better counteract perturbations at the Moon. The power required for 1 mN of thrust is within maximum power available for the propulsion system and it was assumed as maximum thrust possible with constraints of power assumed.

6 Conclusion

With an accelerator electrode the electrospray propulsion technology gains also the feature of tailoring thrust, specific impulse and power consumption (see Subsection 4.3). This flexibility is a desirable property of any propulsion system.

In parallel, LLO are of interest because of the vicinity with the Moon's surface that could allow a more accurate exploration of the Moon; polar orbits are instead of interest because of presence of water. Because of that, low lunar quasi-circular polar orbits were studied and, thanks to the polar maps that were created, it has been understood that these kinds of orbits are extremely perturbed. Without a careful choice of the initial orbit or without a propulsion system able to maintain the initial orbit in time, the satellite might impact the Moon in few months. The stability of LLO was studied by representing maps showing the total variation of orbital elements over 70 days and varying eccentricity and inclination values for a limited set of orbital parameters.

Acknowledgments

The work performed for this paper on the orbital dynamics and control has received funding from the European Research Council (ERC) under the European Union's Horizon 2020 research and innovation programme (grant agreement No 679086 –COMPASS).

References

[1] http://www.vacco.com/space/overview, (Last accessed 20.03.2017)
[2] http://www.busek.com/cubesatprop main.htm, (Last accessed 20.03.2017)
[3] http://www.accion-systems.com/ (Last accessed 20.03.2017)
[4] http://www.enpulsion.com (Last accessed 20.03.2017)

[5] J. Mueller, R. Hofer, and J. Ziemer, Survey of propulsion technologies applicable to CubeSat. 2010.
[6] M. M. Sanchez and P. Lozano, 16 522 Space Propulsion, 2015, https://ocw.mit.edu, (Last accessed 20.03.2017)
[7] D. Courtney, S. Dandavino, and H. Shea, Comparing Direct and Indirect Thrust Measurements from Passively Fed Ionic Electrospray Thrusters, Journal of Propulsion and Power 32.2 (2015), pp. 392–407.
[8] D. Courtney and H. Shea, Influences of porous reservoir Laplace pressure on emissions from passively fed ionic liquid electrospray sources, Applied Physics Letters 107.10 (2015), p. 103504.
[9] Ziemer J. K., Randolph T. M., Franklin G. W., Hruby V., Spence D., Demmons N., Roy T., Ehrbar E., Zwahlen J., Martin R., Connolly W., "Delivery of Colloid Micro-Newton Thrusters for the Space Technology 7 Mission", 44th AIAA/ASME/SAE/ASEE Joint Propulsion Conference and Exhibit, 21-23 July 2008, Hartford, CT. AIAA 2008-4826.
[10] P. E. Clark et al., Lunar Ice Cube Mission: Determining Lunar Water Dynamics with a First Generation Deep Space CubeSat, Science 330 (2016), pp. 463–468.
[11] D. Folta and D. Quinn, Lunar Frozen Orbits, Astrodynamics Specialist Conference and Exhibit, Keystone, Colorado, August 21-24 2006.
[12] M. Lara, Design of long-lifetime lunar orbits, a hybrid approach, *Acta Astronautica* 69 (2011), pp. 186–199.
[13] A. D. Perez, Lunar orbit stability for Small Satellite mission design, Interplanetary CubeSat Workshop, NASA Ames Research Center, May 26-27 2015.
[14] C. Colombo, Planetary Orbital Dynamics (PlanODyn) suite for long term propagation in perturbed environment, 6th International Conference on Astrodynamics Tools and Techniques (ICATT). 2016, pp. 14–17.
[15] C. Colombo et al., End-of-life Earth re-entry for highly elliptical orbits: the INTEGRAL mission, The 24th AAS/AIAA Space Flight Mechanics Meeting. 2014, pp. 26–30.
[16] C. Colombo and C. McInnes, Orbital Dynamics of "Smart-Dust" Devices with Solar Radiation Pressure and Drag, Journal of Guidance, Control and Dynamics 34.6 (2011), pp. 1613–1631.
[17] C. Colombo et al., End-of-life disposal concepts for Libration Point Orbit and Highly Elliptical Orbit missions, *Acta Astronautica* 110 (2015), pp. 298–312.
[18] P. O. Hayne et al., Lunar Flashlight: Mapping Lunar Surface Volatiles Using a CubeSat, Annual Meeting of the Lunar Exploration Analysis Group, Vol. 1748. LPI Contributions. Oct. 2013, p. 7045.
[19] The CuSP interplanetary CubeSat mission, 2016, http://mstl.atl.calpoly.edu/~bklofas/Presentations/DevelopersWorkshop2016/4_DonGeorge.pdf, (Last accessed 20.03.2017)
[20] J. Harbaugh, ed. LunaH-Map: University-Built CubeSat to Map Water-Ice on the Moon, 2016, https://www.nasa.gov/feature/lunah- map-university-built-cubesat-to-map-water-ice-on-the-moon,(accessed 20.03.2017)
[21] C. Hardgrove et al., The Lunar Polar Hydrogen Mapper (LunaH-Map) Cube-Sat Mission, Lunar and Planetary Science Conference, Vol. 47. Lunar and Planetary Inst. Technical Report. Mar. 2016, p. 2654.
[22] Y. Kovo, ed. BioSentinel, 2016, https://www.nasa.gov/centers/ames/engineering/projects/biosentinel.html, (accessed 20.03.2017)
[23] N. Namiki et al, Farside gravity field of the Moon from four-way Doppler measurements of SELENE (Kaguya), Science 323.5916 (2009), pp. 900–905.
[24] A. S. Konopliv et al., Recent gravity models as a result of the Lunar Prospector mission, Icarus 150.1 (2001), pp. 1–18.
[25] A. Ruggiero et al., Low-thrust maneuvers for the efficient correction of orbital elements, 32nd International Electric Propulsion Conference. 2011, pp. 11–15.
[26] P. E. Clark, W. Holemans, and W. Bradley, Lunar Water Distribution (LWaDi)–a 6U Lunar Orbiting spacecraft SSC14-WK-22, http://mstl.atl.calpoly.edu/~workshop/archive/2014/Summer/Day%202/0920%20-%20Clark%20-%20Lunar%20Water%20Distribution%20(LWaDi).pdf, (Last accessed 05/09/2017).
[27] D. Courtney, S. Dandavino, and H. Shea, Comparing Direct and Indirect Thrust Measurements from Passively Fed Ionic Electrospray Thrusters, Journal of Propulsion and Power 32.2 (2015), pp. 392–407.
[28] D. Courtney and H. Shea, Influences of porous reservoir Laplace pressure on emissions from passively fed ionic liquid electrospray sources, Applied Physics Letters 107.10 (2015), p. 103504.
[29] M. Lara, B. De Saedeleer, and S. Ferrer, Preliminary design of low lunar orbits, Proceedings of the 21st International Symposium on Space Flight Dynamics. 2009, pp. 1–15.
[30] H. D. Curtis. Orbital mechanics for engineering students. Butterworth-Heinemann, 2013.
[31] S. Dandavino et al., Microfabricated electrospray emitter arrays with integrated extractor and accelerator electrodes for the propulsion of small spacecraft, Journal of Micromechanics and Microengineering 24.7 (2014), p. 075011.

[32] P. Lozano, Studies on the ion-droplet mixed regime in colloid thrusters, PhD thesis, Yale University, 2003.
[33] M. Benetti, Feasibility on an electrospray propulsion system for a 6U CubeSat to the Moon, MSc thesis, Politecnico di Milano, 2017, Supervirors: Dr. C. Colombo, Dr. C. Ryan.
[34] Legge J. R. S., "Finite Element Modelling of Ionic Liquid Flow Through Porous Electrospray Emitters", Final Project, M.I.T., project number 18.086, http://math.mit.edu/classes/18.086/2008/final_report_robert_legge.pdf (Last accessed 06/09/2017).